

Article

Tuning the Crystal Habits of Organic Explosives by Antisolvent Crystallization: The Case Study of 2,6-dimaino-3,5-dinitropyrazine-1-oxid (LLM-105)

Xiaoqing Zhou ¹, Junhui Shan ², Dong Chen ¹ and Hongzhen Li ^{1,*}¹ Institute of Chemical Materials, China Academy of Engineering Physics, Mianyang 621900, China² School of Environment and Safety Engineering, North University of China, Taiyuan 030051, China

* Correspondence: hongzhenli@caep.cn; Tel.: +86-0816-2480352

Received: 29 June 2019; Accepted: 17 July 2019; Published: 30 July 2019



Abstract: Crystallization is one of the most important methods in the crystal habit control of explosive products. For this study, the antisolvent crystallization experiments were carried out to tune the crystal habits of 2,6-dimaino-3,5-dinitropyrazine-1-oxid (LLM-105). Dimethyl sulphoxide (DMSO) was used as an organic solvent. Water, methanol, acetic acid, nitromethane, acetone, ethanol, methylene chloride, o-dichlorobenzene, and toluene were selected as antisolvents. The X-shaped, spherical cluster-like, rod-like, needle-like, and dendritic crystals were successfully produced by varying the kind of the antisolvent. These results manifested that the polarity and functional groups of antisolvent molecules played important roles in the crystal habits of LLM-105 explosive. The powder X-ray diffraction (PXRD) and Fourier transform infrared (FT-IR) measurements indicated that these antisolvents just tuned the crystal habit of LLM-105 but did not change the crystal structure. The differential scanning calorimetry (DSC) and thermogravimetry (TG) results of the obtained crystals showed that the crystal habits significantly affected the thermal properties. This study can contribute to the investigation of the mechanism of antisolvent-induced crystal habit modification and screen out the efficient antisolvents.

Keywords: antisolvent crystallization; crystal habits; 2,6-dimaino-3,5-dinitropyrazine-1-oxid (LLM-105)

1. Introduction

Crystallization is a widely used technology in the petrochemical, chemical, food, pharmaceutical, and explosive industries [1,2]. Over the past several decades, the development of crystallization methods has been accelerated due to the increasing number of requests for crystals with specific properties [3]. As one of the most important crystal qualities, crystal habit (the characteristic external shape of a crystal) not only has a considerable impact on the physicochemical properties such as dissolution rate, bioavailability, solubility, and compressibility of crystal products, but also significantly affects the downstream operations such as filtration, drying, and milling [4–6]. For explosives, crystal habits are particularly important because they affect the mechanical and safety properties as well as the formulation and manufacturing processes, thus determining the further application of explosive crystals [7–11]. Therefore, in the development of high-quality explosives, it is worth exploring their crystallization strategies to obtain a proper crystal habit.

The crystal habit modification can be induced by changing crystallization conditions such as solvent, temperature, agitating speed, and degree of supersaturation [12,13]. In recent years, advanced strategies have also been employed to modify the crystal habits by adding tailor-made additives such as surfactants, structurally related compounds, and polymers [14–19]. Compared with the utilization

of tailor-made additives, the solution crystallization method by changing the crystallization conditions is more facile. Conventional solution crystallization techniques such as solvent evaporation or cooling crystallization have the disadvantage of being expensive and energy intensive [20]. Because of less energy intensiveness, simplicity, and low setup cost, antisolvent crystallization are traditionally carried out at a predefined constant temperature by adding an antisolvent to a saturated solution of a solute in a solvent. It is widely used in heat sensitive substances such as pharmaceutical compounds and explosives [21–24]. The core of antisolvent crystallization is the selection of a suitable antisolvent that can decrease the solubility of a solute in the solution and promote precipitation. The physical and chemical properties of the antisolvent directly influence the rate of mixing with the solution, thereby affecting the nucleation and growth of the crystals and the final crystal habit. In addition, the conditions involved in crystallization experiments such as the amount of antisolvent used, anti-solvent addition rate, and location of addition of antisolvent, also strongly affect the crystal formation mechanism and govern the resulting crystal shape and size. Although the antisolvent has a direct and substantial impact on the crystal habits, the effect of antisolvent is still unclear. One reason for the influence on the crystal habits caused by the antisolvent can be explained by the interactions between the solute and the antisolvent. For example, the antisolvent interacts strongly with the solute mostly by hydrogen bonds, which was caused by the intrinsic polarity of the solvent used, increasing its strength so that the system is forced to crystallize [25]. For the antisolvent crystallization technology, understanding the effect of the antisolvent on the crystal morphology will help to design and select an appropriate antisolvent to obtain the product with desired crystal habits.

The main objective of the present work is to investigate the influence of antisolvents on the crystal habits of organic explosives produced by antisolvent crystallization. In this study, 2,6-diamino-3,5-dinitropyrazine-1-oxide (LLM-105) was chosen as a model organic explosive due to its absence of polymorphism, thus making it easier to attribute the changes of crystal habit to the crystallization conditions. LLM-105 is a typical high energetic and insensitive explosive, which was first described by Pagoria and coworkers in 1998 [26]. Because of its excellent thermal stability and safety, LLM-105 has potential applications in specialty munitions and civil fields [27]. As depicted in Figure 1a, the molecular structure contains nitro and amino groups, resulting in strong intermolecular and intramolecular hydrogen bonds interactions. It has a wave-like layered arrangement within a monoclinic structure [28,29]. The π -bond, strong intramolecular, and intermolecular hydrogen bonds might be responsible for the extraordinary thermal stability and safety. In addition, LLM-105 exhibits a very low solubility in most organic solvents due to these strong hydrogen bonds, which facilitates the choice of antisolvents. Although some papers have been published on the crystallization of LLM-105, relatively few literatures have reported the antisolvent crystallization [30–33]. Only few antisolvents such as water and ethyl acetate have been involved, and there is still no clear explanation for the effect of antisolvents on the morphology of LLM-105. In this paper, dimethyl sulphoxide (DMSO) was used as an organic solvent, and nine antisolvents (Figure 1b–j) with different polarity index (PI) were employed to carry out the antisolvent crystallization experiments of LLM-105. The same crystallization parameters as LLM-105 concentration, solvent to antisolvent ratio, crystallization temperature, and injection rate have been employed to observe the influence of antisolvent on crystal habits. Powder X-ray diffraction (PXRD), Fourier transform infrared (FTIR), and scanning electron microscopy (SEM) were used to characterize the structure and morphology. Differential scanning calorimetry (DSC) and thermogravimetry (TG) measurements were performed to analyze the influence of crystal habits on the thermal properties of LLM-105.

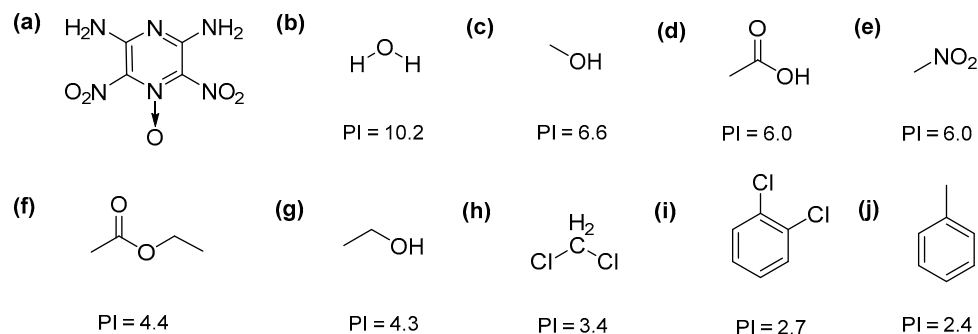


Figure 1. Molecular structures of (a) 2,6-diamino-3,5-dinitropyrazine-1-oxide (LLM-105), (b) H₂O, (c) CH₃OH, (d) CH₃COOH, (e) CH₃NO₂, (f) CH₃COOC₂H₅, (g) C₂H₅OH, (h) CH₂Cl₂, (i) C₆H₄Cl₂, and (j) C₆H₅CH₃.

2. Materials and Methods

2.1. Chemicals

LLM-105 raw materials were synthesized according to the reported method [26]. Analytical dimethyl sulfoxide (DMSO, C₂H₆O_S), methanol (MeOH, CH₃OH), acetic acid (AcOH, CH₃COOH), nitromethane (NM, CH₃NO₂), ethyl acetate (EAC, CH₃COOC₂H₅), ethanol (EtOH, C₂H₅OH), methylene chloride (MC, CH₂Cl₂), o-dichlorobenzene (DCC, C₆H₄Cl₂), and toluene (TL, C₆H₅CH₃) were purchased from Chengdu United Chemical industry (Chengdu, China). The distilled water (H₂O) was obtained by using a Milli-Q apparatus (Millipore, Bedford, MA, USA).

2.2. Antisolvent Crystallization Experiments

In order to investigate the effect of antisolvents on the crystal habits of LLM-105, nine antisolvents with different polarity and active groups were selected. Water, methanol, acetic acid, nitromethane, ethyl acetate, alcohol, methylene chloride, o-dichlorobenzene, and toluene were used as antisolvents. The polarity index (PI) of the nine antisolvents is different, which is related to the strength of the hydrogen bond. The higher the polarity, the stronger the hydrogen bond [34,35]. The antisolvent crystallization experiments of LLM-105 were performed in a stirred glass crystallizer, the speed of the magnetic stirrer was 300 rpm. On the basis of the solubility data of LLM-105 [36], LLM-105 raw materials were dissolved into DMSO to obtain a saturated solution with a concentration of 0.03 g/mL. The saturated solution of LLM-105 was heated to 10 °C above the saturation temperature for 30 min to ensure that no crystal nuclei remained in the solution. Then the solution was cooled to 30 °C and maintained at this temperature. Subsequently, the antisolvent was fed to LLM-105 saturated solutions in a volume ratio of 3:1 (antisolvent:solvent), and the feed rate of antisolvent was 5 mL·min⁻¹. All the experiments were conducted with the same parameters as LLM-105 concentration, solvent to antisolvent ratio, crystallization temperature, and antisolvent feed rate. For each antisolvent, three experiments using the same crystallization parameters were carried out to validate the reproducibility of the results. After the crystals precipitated, the solution was stirred for 30 min. Then the crystals were filtered, washed with distilled water, and dried in a vacuum drying chamber at 80 °C for 4 h.

2.3. Characterization

Powder X-ray diffraction (XRD, Bruker, Ettlingen, Germany) patterns were recorded to determine the crystalline changes and polymorphic transformations using D8 advance, Bruker with Cu K α radiation detector ($\lambda = 1.5418 \text{ \AA}$) filter at a voltage of 40 kV and a current of 30 mA. Fourier transform infrared (FTIR, Thermo Scientific, Logan, UT, USA) spectra were recorded from 400 to 4000 cm⁻¹. The FTIR data were collected in the crystalline state via KBr pellets. Scanning electron microscopy (SEM, Sigma-HD, Zeiss, Jena, Germany) was used to analyze the morphology of the LLM-105 crystals obtained from different antisolvents. Differential scanning calorimetry (DSC-1, Mettler Toledo, Zurich,

Swiss) and thermogravimetry (TGA851, Mettler Toledo, Zurich, Swiss) measurements were carried out from 50 °C to 500 °C with a heating rate of 10 °C·min⁻¹ at a flow rate of 40 mL·min⁻¹ under N₂ atmosphere.

3. Results and Discussion

3.1. Influence of Antisolvent on the Crystal Habit

In order to investigate the influence of antisolvent on the crystal habits of LLM-105, the same crystallization parameters as LLM-105 concentration, solvent to antisolvent ratio, crystallization temperature, and injection rate were employed in each experiment. Taking into account the polarity and active groups of the antisolvent, we used water, methanol, acetic acid, nitromethane, ethyl acetate, alcohol, methylene chloride, o-dichlorobenzene, and toluene as antisolvents. Moreover, to validate the reproducibility of the results, three crystallization experiments were performed for each antisolvent. The results showed that the crystals obtained from the same antisolvent exhibited the same habit. The SEM images of LLM-105 crystals obtained from different antisolvents are shown in Figure 2, indicating that the crystals of LLM-105 prepared via antisolvent crystallization retain their crystal structural integrity. However, the morphology of particles obtained from different antisolvents showed obvious dissimilarity, which suggested that the antisolvents have shown significant effect on the morphology of LLM-105 crystals. We noticed that the crystals crystallized from water (PI = 10.2), were X-shaped (Figure 2a). The strong polar antisolvent, such as methanol (PI = 6.6) and acetic acid (PI = 6.0) tended to provide crystals with spherical clusters (Figure 2b,c). However, the appearance and morphology of crystals obtained from nitromethane, which is also a strong polar antisolvent with the same PI as acetic acid, was rod-shaped (Figure 2d). When the polarity of the antisolvent was medium (ethyl acetate, PI = 4.4, and ethanol, PI = 4.3, and methylene chloride, PI = 3.4), the crystals became needle-like, and as the antisolvent PI decreased, the length to diameter ratio of crystals decreased (Figure 2e–g). When the antisolvent was methylene chloride (PI = 3.4), short and flat rod-like crystals were produced. In particular, using small polar o-dichlorobenzene (PI = 2.7) and toluene (PI = 2.4) as antisolvents, dendritic crystals appeared (Figure 2h,i).

In this study, the polarity of the antisolvent is one of the most vital properties that may affect the habit of the LLM-105 crystals. This can be explained by the antisolvent–solute interactions. The antisolvents can be absorbed to different surfaces of LLM-105 by the intermolecular interactions between the antisolvent molecules and LLM-105 molecules, thereby affecting the nucleation and growth of the crystal, and resulting in morphological changes of the final crystal. The nine antisolvents differ by polarity index, which is related to the hydrogen bonds with higher polarity implying stronger hydrogen bonds. It is speculated that under the same crystallization conditions, the higher the anti-solvent polarity, the stronger the intermolecular interaction. Since the polarity of methanol is stronger than ethanol, the growth of the crystal from the needle direction was inhibited and spherical cluster-like crystals were formed. From Figure 2b,c, it can be concluded that in addition to the polarity, the functional groups of antisolvent molecules are also important factors influencing the crystal morphology. The results highlighted the ability of antisolvents to tune the crystal habits of LLM-105 crystals. The morphology and size of the LLM-105 crystals can be tailored by an antisolvent with proper polarity and active groups.

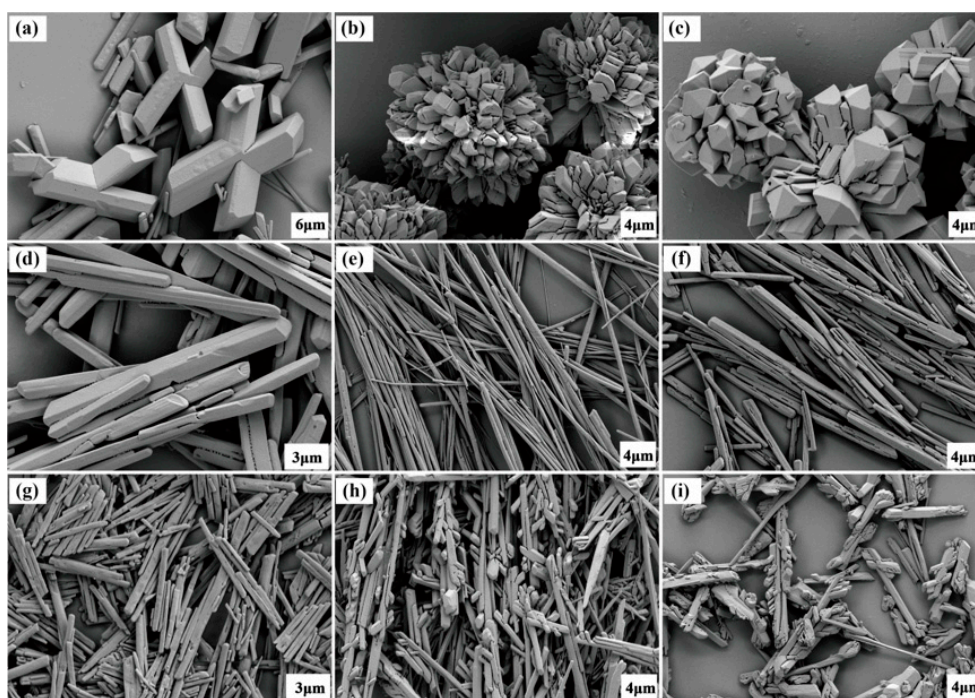


Figure 2. Scanning electron microscopy (SEM) images of LLM-105 crystals obtained by varying antisolvent. (a) Water, (b) methanol, (c) acetic acid, (d) nitromethane, (e) ethyl acetate, (f) ethanol, (g) methylene chloride, (h) o-dichlorobenzene, and (i) toluene.

3.2. Structural Characterization of LLM-105 Crystals

The crystal structure of LLM-105 was confirmed by powder XRD patterns. As shown in Figure 3, the powder diffraction patterns of the LLM-105 crystals obtained from different antisolvents exhibit good agreement with the simulation results, which confirmed that all the crystals with different morphologies are in the same monoclinic crystal structure. However, the peak intensities at $2\theta = 12.1^\circ$, 22.2° , and 28.4° of LLM-105 were significantly different. The diffraction peaks at $2\theta = 12.1^\circ$, 22.2° , and 28.4° are assigned to those from the (011), (012), and (14-1) planes, respectively. It is suggested that the relative area of the {011}, {012}, and {14-1} facets in the crystals is different. It can be noted that the peak intensity of long needle-like crystals obtained from ethyl acetate was significantly different from that of other crystals. For long needle-like crystals, a decrease in peak intensity of (14-1) plane and an increase in peak intensity of (011) and (012) planes were observed. The strongest peak of long needle-like crystals was (012) plane, while that of other crystals was (14-1) plane. In these cases, it was seen that only the change in crystal habit occurred. These results indicate that the antisolvents just tune the crystal habit of LLM-105, but do not lead to the polymorphism change.

FT-IR spectroscopy of LLM-105 was carried out to further characterize the LLM-105 structure. As shown in Figure 4, FT-IR spectra of all LLM-105 crystals obtained from different antisolvents showed the same characteristic bands of the $-\text{NO}_2$ and $-\text{NH}_2$ functional groups with wavenumber ranges in the $1489\text{--}1642\text{ cm}^{-1}$ and $3229\text{--}3433\text{ cm}^{-1}$ regions, respectively, together with numerous peaks in the fingerprint region. The results of FTIR spectra analysis also confirmed that no polymorphic changes occurred. Also, the FTIR results clearly showed that solvents were not incorporated into the crystal structure. The results suggested that the antisolvents were not incorporating themselves into the crystals, but instead affected the crystallization process itself. They could influence the different kinetic growth of the crystal faces because of the different velocity of dissolution of the antisolvents in the solution, and thereby affecting the habits.

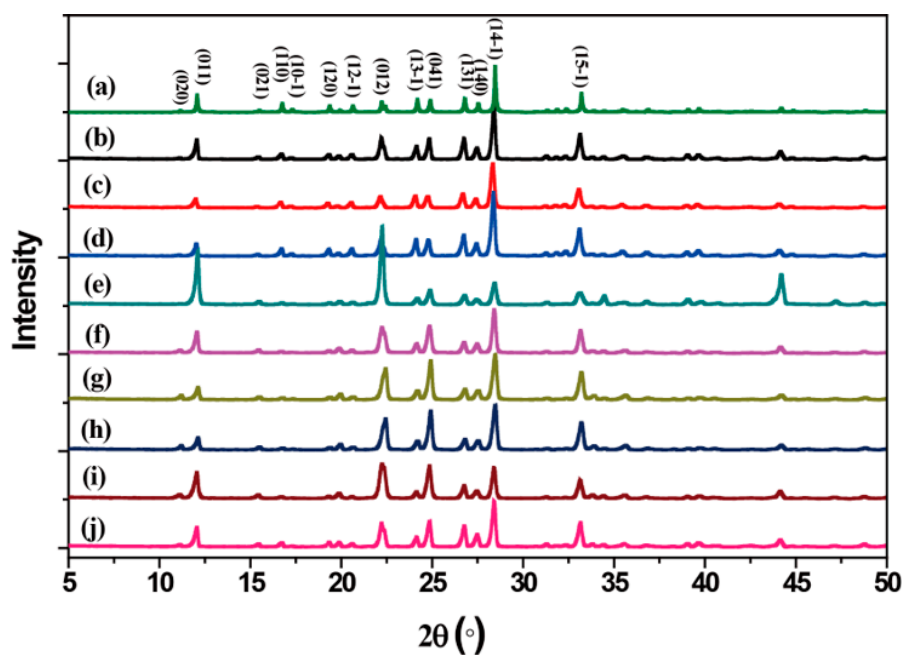


Figure 3. Powder X-ray diffraction patterns of (a) simulated, and (b–j) different shaped LLM-105 crystals obtained from varying antisolvent. (b) Water, (c) methanol, (d) acetic acid, (e) nitromethane, (f) ethyl acetate, (g) ethanol, (h) methylene chloride, (i) o-dichlorobenzene, and (j) toluene.

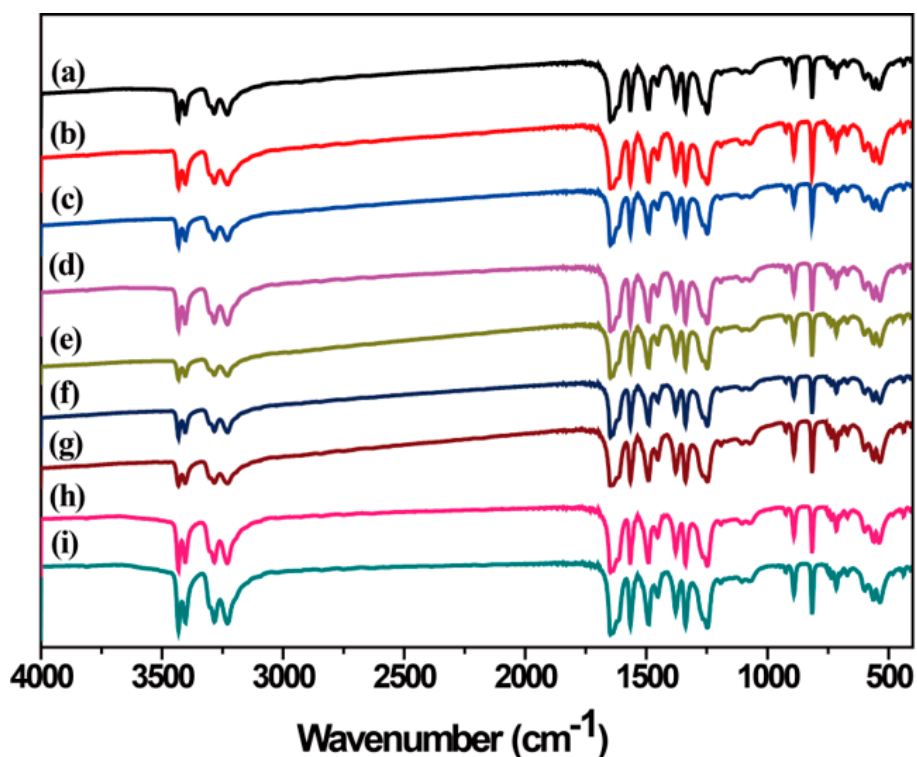


Figure 4. Fourier transform infrared (FTIR) spectra of LLM-105 crystals obtained from different antisolvents. (a) Water, (b) methanol, (c) acetic acid, (d) nitromethane, (e) ethyl acetate, (f) ethanol, (g) methylene chloride, (h) o-dichlorobenzene, and (i) toluene.

3.3. Thermal Properties of LLM-105 Crystals

For explosives, especially for LLM-105, thermal properties are important for practical applications. One of the most important potential applications of LLM-105 is as initiated explosives in slapper detonators due to its excellent thermal and shock stability. Therefore, the exothermic reactions of LLM-105 crystals are one of the most significant thermal properties in the current study. In order to study the influence of crystal habits in the thermal properties of the crystals obtained from different antisolvents, differential scanning calorimetry (DSC) and thermogravimetry (TG) measurements were carried out with a heating rate of $10\text{ }^{\circ}\text{C}\cdot\text{min}^{-1}$ at a flow rate of $40\text{ mL}\cdot\text{min}^{-1}$ under N_2 atmosphere. The DSC and TG curves are shown in Figures 5 and 6, respectively. Table 1 summarizes the initial decomposition temperatures, exothermic peaks, and the final decomposition temperatures of the crystals obtained from different antisolvents.

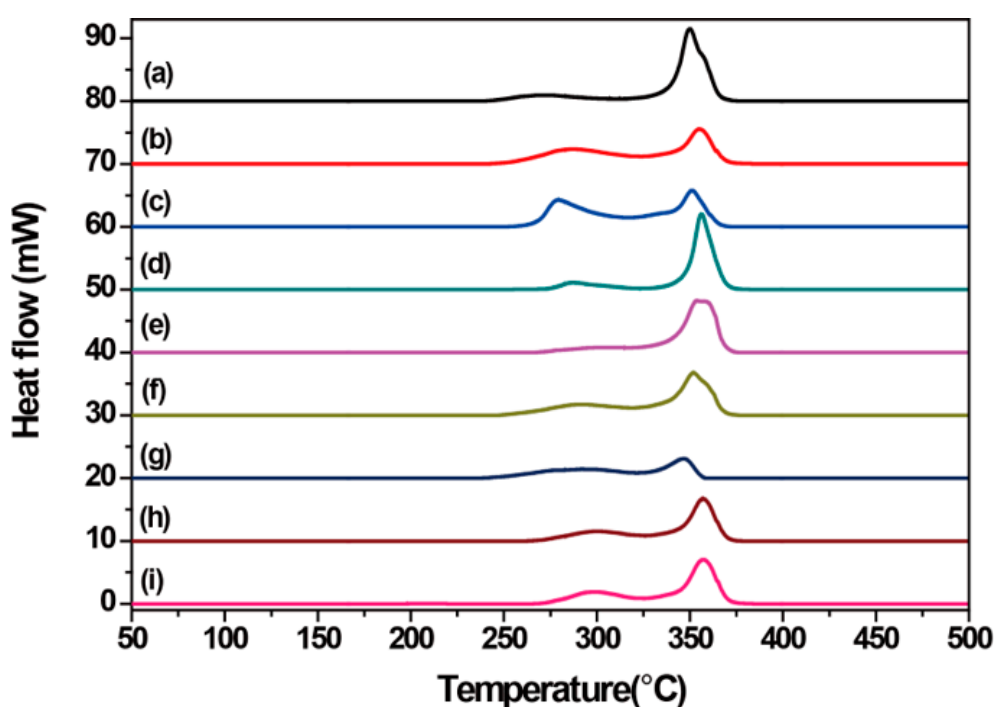


Figure 5. Differential scanning calorimetry (DSC) curves of LLM-105 crystals obtained from different antisolvents. (a) Water, (b) methanol, (c) acetic acid, (d) nitromethane, (e) ethyl acetate, (f) ethanol, (g) methylene chloride, (h) o-dichlorobenzene, and (i) toluene.

Table 1. Thermal analysis of LLM-105 crystals obtained from different antisolvents.

Antisolvent	H ₂ O	MeOH	AcOH	NM	EAC	EtOH	MC	DCC	TL
T_1 (°C)	252.1	252.6	259.2	263.9	271.7	259.9	259.6	270.6	271.9
T_2 (°C)	270.0	286.8	279.3	287.3	309.8	292.8	292.3	301.0	299.8
T_3 (°C)	349.7	355.2	351.0	356.3	353.8	351.8	346.3	357.2	357.0
T_4 (°C)	362.3	366.7	363.2	366.8	366.7	364.8	360.4	366.6	366.6

T_1 : The initial decomposition temperature; T_2 : The first exothermal peak; T_3 : The second exothermal peak; T_4 : The final decomposition temperature.

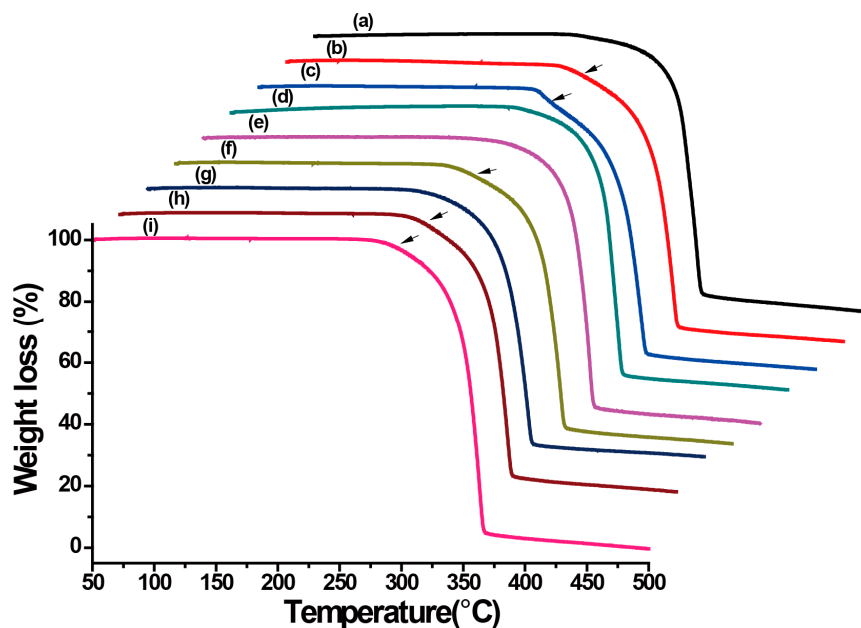


Figure 6. Thermogravimetry (TG) curves of LLM-105 crystals obtained from different antisolvents. (a) Water, (b) methanol, (c) acetic acid, (d) nitromethane, (e) ethyl acetate, (f) ethanol, (g) methylene chloride, (h) o-dichlorobenzene, and (i) toluene.

DSC results demonstrated that the thermal properties of crystals obtained from water (Figure 5a), nitromethane (Figure 5d), ethyl acetate (Figure 5e), and methylene chloride (Figure 5g) are significantly different than those obtained from methanol (Figure 5b), acetic acid (Figure 5c), ethanol (Figure 5f), o-dichlorobenzene (Figure 5h), and toluene (Figure 5i). The former clearly showed a very slow initial exothermic process. The TG curves also confirmed this difference of the thermal decomposition, as indicated by the arrows (Figure 6). The “dimple” on the TG curves was clearly visible for Figure 6b,c,f,h,i, but not apparent for Figure 6a,d,e,g. From the DSC and TG curves, two exothermic decomposition stages of all LLM-105 crystals were observed. The first exothermic decomposition processes occurred in a broad temperature range (252.1–325.0 °C) and the second exothermic decomposition processes were focused in a narrow temperature range (325.0–366.7 °C). As for the first exothermic decomposition stage, the initial decomposition temperatures of the long needle-like crystals obtained from ethyl acetate and the dendritic crystals obtained from o-dichlorobenzene and toluene were above 270.0 °C. It can be noted that the crystals obtained from water, ethyl acetate, and dichloromethane slowly decomposed, while the crystals obtained from other antisolvents decomposed faster. Especially for the spherical cluster-like crystals (Figure 5b,c) and the dendritic crystals (Figure 5h,i), their exothermic peaks were particularly noticeable. It can be clearly observed that the first exothermic peaks of LLM-105 crystals strongly depend on the crystal habits. The X-shaped crystals obtained from water exhibited the lowest exothermic peak at 270.0 °C (first exothermic peak), while the long needle-like crystals obtained from ethyl acetate showed the highest exothermic peak at 309.8 °C (first exothermic peak). The dendritic crystals obtained from o-dichlorobenzene and toluene also displayed strong exothermic peak at 301.0 °C and 299.8 °C, respectively. As for the second exothermic decomposition stage, the exothermic peak of the dendritic crystals obtained from o-dichlorobenzene and toluene was 357.0 °C and 357.2 °C, respectively. Both of them are higher than that of the crystals obtained from the other antisolvents. The short and flat rod-like crystals obtained from methylene chloride showed a lowest exothermic peak at 346.3 °C (second exothermic peak), which was about 10 °C lower than the fractal growth crystals. In all cases, the final decomposition temperature of the crystals obtained from these antisolvents was above 360 °C, and no significant difference of the final decomposition temperature was observed. The results show that the crystal morphologies significantly affect the thermal properties of the LLM-105 crystals.

4. Conclusions

The crystal habit control of LLM-105 has been studied by the antisolvent crystallization method using DMSO as the organic solvent. In this study, nine antisolvents such as water, methanol, acetic acid, nitromethane, acetone, ethanol, methylene chloride, o-dichlorobenzene, and toluene were used to investigate their effects on the crystal morphology. In the case of other crystallization conditions being the same, the crystal habit of LLM-105 was strongly dependent on the antisolvent. LLM-105 crystals with different crystal habits such as X-shaped, spherical cluster-like, rod-like, needle-like, and dendritic samples were successfully produced by varying the kind of the antisolvent. The results suggested that the polarity and functional groups of the antisolvent molecules played important roles on the morphology of the LLM-105 crystals. The morphology and size of the LLM-105 crystals can be tailored by this simple antisolvent crystallization method via choosing a proper antisolvent. The crystal structure of LLM-105 was confirmed by PXRD and FT-IR, and the results indicated that these antisolvents just tuned the crystal habit of LLM-105 but did not change the crystal structure. In addition, the thermal properties of the obtained LLM-105 crystals were also investigated. It can be concluded that the crystal morphologies significantly affect the thermal properties of LLM-105 crystals. The results are useful to deepen the understanding of the crystal habit modification of organic explosives.

Author Contributions: Conceptualization, X.Z., J.S., D.C. and H.L.; data curation, J.S.; investigation, X.Z.; supervision, J.S. and D.C.; visualization, X.Z.; writing—original draft, X.Z.; writing—review and editing, H.L.

Funding: This research was funded by the National Natural Science Foundation of China (11302199 and 11672273).

Conflicts of Interest: The authors declare no conflict of interest.

References

1. Wu, H.; Dong, Z.; Li, H.; Khan, M. An Integrated Process Analytical Technology (PAT) Approach for Pharmaceutical Crystallization Process Understanding to Ensure Product Quality and Safety: FDA Scientist's Perspective. *Org. Process Res. Dev.* **2015**, *19*, 89–101. [[CrossRef](#)]
2. Mandal, A.K.; Thanigaivelan, U.; Pandey, R.K.; Asthana, S.; Khomane, R.B.; Kulkarni, B.D. Preparation of Spherical Particles of 1,1-Diamino-2,2-dinitroethene (FOX-7) Using a Micellar Nanoreactor. *Org. Process Res. Dev.* **2012**, *16*, 1711–1716. [[CrossRef](#)]
3. Desiraju, G.R. Crystal engineering: From molecule to crystal. *J. Am. Chem. Soc.* **2013**, *135*, 9952–9967. [[CrossRef](#)] [[PubMed](#)]
4. Lee, A.Y.; Erdemir, D.; Myerson, A.S. Crystal Polymorphism in Chemical Process Development. *Annu. Rev. Chem. Biomol. Eng.* **2011**, *2*, 259–280. [[CrossRef](#)]
5. Mugheirbi, N.A.; Tajber, L. Crystal Habits of Itraconazole Microcrystals: Unusual Isomorphic Intergrowths Induced via Tuning Recrystallization Conditions. *Mol. Pharm.* **2015**, *12*, 3468–3478. [[CrossRef](#)]
6. Iohara, D.; Yoshida, K.; Yamaguchi, K.; Anraku, M.; Motoyama, K.; Arima, H.; Uekama, K.; Hirayaa, F. Cyclodextrin-Induced Change in Crystal Habit of Acetylsalicylic Acid in Aqueous Solution. *Cryst. Growth Des.* **2012**, *12*, 1985–1991. [[CrossRef](#)]
7. Van der Steen, A.C.; Verbeek, H.J.; Meulenbrugge, J.J. Influence of RDX crystals shape on the shock sensitivity of PBXs. In Proceedings of the 9th International Detonation Symposium on Detonation, Portland, OR, USA, 28 August–1 September 1989.
8. Boddu, V.M.; Viswanath, D.S.; Ghosh, T.K. Damavarapu, 2,4,6-Triamino-1,3,5-trinitrobenzene (TATB) and TATB-based formulations—A review. *J. Hazard. Mater.* **2010**, *181*, 1–8. [[CrossRef](#)] [[PubMed](#)]
9. Li, J.; Wu, S.; Lu, K. Study on Preparation of Insensitive and Spherical High Bulk Density Nitroguanidine with Controllable Particle Size. *Propellants Explos. Pyrotech.* **2016**, *41*, 312–320. [[CrossRef](#)]
10. Zhang, C.; Peng, Q.; Wang, L.; Wang, X. Thermal Sensitivity of HMX Crystals and HMX-Based Explosives Treated under Various Conditions. *Propellants Explos. Pyrotech.* **2010**, *35*, 561–566. [[CrossRef](#)]
11. Wang, J.; Wang, Y.Q.; Qiao, Z.Q.; Zhang, L.; Wu, P.; Yang, G.C. Self-assembly of TATB 3D architectures via micro-channel crystallization and a formation mechanism. *CrystEngComm* **2016**, *18*, 1953–1957. [[CrossRef](#)]

12. Berkovitch-Yellin, Z.; Van Mil, J.; Addadi, L.; Idelson, M.; Lahav, M.; Leiserowitz, L. Crystal morphology engineering by “tailor-made” inhibitors; a new probe to fine intermolecular interactions. *J. Am. Chem. Soc.* **1985**, *107*, 3111–3122. [[CrossRef](#)]
13. Carstensen, J.T.; Ertell, C.; Geoffroy, J.M. Physico-chemical properties of particulate matter. *Drug Dev. Ind. Pharm.* **1993**, *19*, 195–219. [[CrossRef](#)]
14. Kim, J.-W.; Park, J.-H.; Shim, H.-M.; Koo, K.-K. Effect of amphiphilic additives on nucleation of hexahydro-1,3,5-trinitro-1,3,5-triazine. *Cryst. Growth Des.* **2013**, *13*, 4688–4694. [[CrossRef](#)]
15. Bodnar, K.; Hudson, S.P.; Rasmuson, Å.C. Stepwise use of additives for improved control over formation and stability of mefenamic acid nanocrystals produced by antisolvent precipitation. *Cryst. Growth Des.* **2017**, *17*, 454–466. [[CrossRef](#)]
16. Chen, J.; Ormes, J.D.; Higgins, J.D.; Taylor, L.S. Impact of Surfactants on the Crystallization of Aqueous Suspensions of Celecoxib Amorphous Solid Dispersion Spray Dried Particles. *Mol. Pharm.* **2015**, *12*, 533–541. [[CrossRef](#)]
17. Poornachary, S.K.; Han, G.; Kwek, J.W.; Chow, P.S.; Tan, R.B.H. Crystallizing micronized particles of a poorly water-soluble active pharmaceutical ingredient: Nucleation enhancement by polymeric additives. *Cryst. Growth Des.* **2016**, *16*, 749–758. [[CrossRef](#)]
18. Schram, C.J.; Beaudoin, S.P.; Taylor, L.S. Impact of Polymer Conformation on the Crystal Growth Inhibition of a Poorly Water Soluble Drug in Aqueous Solution. *Langmuir* **2015**, *31*, 171–179. [[CrossRef](#)]
19. Verma, V.; Peddapatla, R.V.G.; Crowley, C.M.; Crean, A.M.; Davern, P.; Hudson, S.; Hodnett, B.K. Experimental study on the influence of excipients on the heterogeneous crystallization and dissolution properties of an active pharmaceutical ingredient. *Cryst. Growth Des.* **2018**, *18*, 338–350. [[CrossRef](#)]
20. Thorson, M.R.; Goyal, S.; Gong, Y.; Zhang, G.G.Z.; Kenis, P.J.A. Microfluidic approach to polymorph screening through antisolvent crystallization. *CrystEngComm* **2012**, *14*, 2404–2412. [[CrossRef](#)]
21. Holaň, J.; Skořepová, E.; Heraud, L.; Baltés, D.; Rohlíček, J.; Dammer, O.; Ridvan, L.; Štěpánek, F. Polymorphic Crystallization and Structural Aspects of Agomelatine Metastable Form X Prepared by Combined Antisolvent/Cooling Process. *Org. Process Res. Dev.* **2016**, *20*, 33–43. [[CrossRef](#)]
22. Tierney, T.B.; Rasmuson, Å.C.; Hudson, S.P. Size and Shape Control of Micron-Sized Salicylic Acid Crystals during Antisolvent Crystallization. *Org. Process Res. Dev.* **2017**, *21*, 1732–1740. [[CrossRef](#)]
23. Kamaraju, V.K.; Chiu, M. Improved Operation of Concentration Control for Antisolvent Crystallization Processes. *Org. Process Res. Dev.* **2015**, *19*, 178–188. [[CrossRef](#)]
24. Bhamidi, V.; Lee, S.H.; He, G.; Chow, P.S.; Tan, R.B.H.; Zukoski, C.F.; Kenis, P.J.A. Antisolvent Crystallization and Polymorph Screening of Glycine in Microfluidic Channels Using Hydrodynamic Focusing. *Cryst. Growth Des.* **2015**, *15*, 3299–3306. [[CrossRef](#)]
25. Cogoni, G.; Baratti, R.; Romagnoli, J.A. On the Influence of Hydrogen Bond Interactions in Isothermal and Nonisothermal Antisolvent Crystallization Processes. *Ind. Eng. Chem. Res.* **2013**, *52*, 9612–9619. [[CrossRef](#)]
26. Pagoria, A.R.; Mitchell, R.D.; Schmidt, R.L.; Simpson, F.; Garcia, J.; Forbes, J.; Cutting, R.; Lee, R.; Swansiger, D.M. Hoffmann, Synthesis, Scale-up and Experimental testing of LLM-105 (2,6-Diamino-3,5-dinitropyrazine-1-oxide). In Proceedings of the Insensitive Munitions and Energetic Materials Technology Symposium, San Diego, CA, USA, 16–19 November 1998.
27. Pagoria, P.; Zhang, M.; Zuckerman, N.; Lee, G.; Mitchell, A.; DeHope, A.; Gash, A.; Coon, C.; Gallagher, P. Synthetic Studies of 2,6-Diamino-3,5-Dinitropyrazine-1-Oxide (LLM-105) from Discovery to Multi-Kilogram Scale. *Propellants Explos. Pyrotech.* **2017**, *42*, 1–14. [[CrossRef](#)]
28. Averkiev, B.B.; Antipin, M.Y.; Yudin, I.L.; Sheremetev, A.B. X-ray Structural Study of Three Derivatives of Dinitropyrazine. *J. Mol. Struct.* **2002**, *606*, 139–146. [[CrossRef](#)]
29. Gilardi, R.D.; Butcher, R.J. 2,6-Diamino-3,5-dinitro-1,4-pyrazine dimethyl sulfoxide solvate. *Crystallogr. Commun.* **2001**, *57*, o757–o759. [[CrossRef](#)]
30. Zhou, X.; Zhang, Q.; Xu, R.; Chen, D.; Hao, S.; Nie, F.; Li, H. A Novel Spherulitic Self-Assembly Strategy for Organic Explosives: Modifying the Hydrogen Bonds by Polymeric Additives in Emulsion Crystallization. *Cryst. Growth Des.* **2018**, *184*, 2417–2423. [[CrossRef](#)]
31. Huang, C.; Liu, J.; Ding, L.; Wang, D.; Yang, Z.; Nie, F. Facile Fabrication of Nanoparticles Stacked 2,6-diamino-3,5-dinitropyrazine-1-oxide (LLM-105) Sub-microspheres via Electrospray Deposition. *Propellants Explos. Pyrotech.* **2018**, *43*, 188–193. [[CrossRef](#)]

32. Zhang, J.; Wu, P.; Yang, Z.J.; Gao, B.; Zhang, J.H.; Wang, P.; Nie, F.D.; Liao, L.Y. Preparation and Properties of Submicrometer-Sized LLM-105 via Spray-Crystallization Method. *Propellants Explos. Pyrotech.* **2014**, *39*, 653–657. [[CrossRef](#)]
33. Bu, R.; Zhou, X.; Li, H.; Yu, Y. Crystallization Metastable Zone of LLM-105 in Dimethyl Sulfoxide. *Chin. J. Energ. Mater.* **2017**, *25*, 479–485.
34. Mirmeharabi, M.; Sohrab, R. An approach to solvent screening for crystallization of polymorphic pharmaceuticals and fine chemicals. *J. Pharm. Sci.* **2005**, *94*, 1560–1576. [[CrossRef](#)] [[PubMed](#)]
35. Vicki, J. Strategies for solvent selection—A literature review. *Trends Anal. Chem.* **1997**, *16*, 293–309.
36. Bu, R.; Zhou, X.; Huang, Q.; Yu, Y.; Li, H. Measurement, Correlation and Thermodynamics of Solubility of 2,6-Diamino-3,5-Dinitropyrazine-1-Oxide (LLM-105) in Eight Solvents. *Propellants Explos. Pyrotech.* **2017**, *42*, 1347–1351. [[CrossRef](#)]



© 2019 by the authors. Licensee MDPI, Basel, Switzerland. This article is an open access article distributed under the terms and conditions of the Creative Commons Attribution (CC BY) license (<http://creativecommons.org/licenses/by/4.0/>).